Dynamic response of quantum dots

V. Shikin,* S. Nazin,* D. Heitmann, and T. Demel
Max-Planck-Institut für Festkörperforschung, Heisenbergstrasse 1, 7000 Stuttgart 80, Federal Republic of Germany
(Received 27 July 1990; revised manuscript received 11 December 1990)

The equilibrium properties and dynamic response of quantum-dot structures with and without magnetic fields are calculated, starting from a confining potential of parabolic shape. Within our analytical theory we can calculate all eigenmodes of the systems. Our calculation can explain the experimentally observed mode spectrum of quantum-dot structures containing about 200 electrons in a disk of radius $R \approx 150$ nm.

I. INTRODUCTION

Currently there is much interest in the investigation of low-dimensional electronic systems derived from originally two-dimensional electronic systems (2DES) in $Al_xGa_{1-x}As/GaAs$ heterostructures or similar systems (see, e.g., Refs. 1–4). Due to an additional lateral confinement, quantum wires (1DES) or quantum dots (0DES) are formed. These systems are called "quantum" structures if this confinement leads to quantized energy levels with level separation larger than kT. For wires, the formation of thus quantized energy levels is usually demonstrated with the method of magnetic-subband depopulation in dc transport experiments.[1] For example, for a 500-nm-wide etched GaAs quantum-wire sample, a typical subband spacing of 2 meV was observed.[5,6] However, use of the dc transport experiment to determine quantization is inherently not possible for dots. Thus optical experiments which measure transitions between levels seem to be a much more direct way to determine the energy spectrum of quantum dots. However, as we will show below, in such experiments also, quantum effects are indicated only very indirectly. The reason for this is that, in most of the currently investigated laterally confined quantum structures,[1–6] the confinement is electrostatic and, as shown in a self-consistent band-structure calculation by Kumar, Laux, and Stern[7] has a nearly parabolic form for the external confining potential. (Also, in etched structures,[3,5,6] the electrons are confined by remote donors in $Al_xGa_{1-x}As$ and negatively charged surface states and are separated by large 200–100-nm-wide depletion regions from the geometrical boundaries. So, in etched structures the confinement is also electrostatic.) Thus a nearly parabolic confinement is a common feature of many known quantum structures. This has important consequences for the optical response.

For an external parabolic confinement, it can be shown, with a rigorous quantum-mechanical calculation, that the dipole excitation always occurs at the eigenfrequency ω_0 determined by the curvature $k = m^*\omega_0^2$ of the external potential.[8,9] The excitation is a rigid center-of-mass motion of all electrons. This result is independent of whether the radius of the dot R is larger or smaller than the effective Bohr radius a_B and independent of the number of electrons, N, as well. (This behavior has actually been observed experimentally by Sikorski and Merkt,[2] which is further experimental justification for the parabolic confinement.) Thus, for an external parabolic potential, the quantum-mechanical excitation is the same as the classical plasma excitation.

In a recent investigation,[3] very small quantum dots with effective electronic radius of $R \approx 100$ nm have been studied which were prepared, starting from $Al_xGa_{1-x}As/GaAs$ heterostructures. The one-particle energy separation of the discrete electron levels was about 2 meV. The optical far-infrared (FIR) response in a perpendicular magnetic field H exhibited a set of magnetoplasmon type of modes (see Refs. 2 and 10–15). In contrast to earlier investigations in semiconductors, a pronounced excitation of two modes by uniform high-frequency electric fields and anticrossing of these modes were observed.[13] The excitation of such higher modes is not allowed in a strictly parabolic confinement; thus in these structures we have nonparabolic terms. The only paper so far available that calculates higher modes is by Fetter.[16] He assumes a 2D disk with an abrupt density profile, i.e.,

$$n(r) = \begin{cases} n_s, & 0 \le r \le R \\ 0, & r > R \end{cases} . \tag{1}$$

Here R is the radius of the disk and n_s the 2D charge density. However, the "abrupt-potential" approximation does not give the experimentally observed mode spacing.

So we present here another ansatz. Based on self-consistent calculations and experimental results, in particular because of the fact that higher modes are very weak,[3] we assume that the parabolic confinement is a good approximation. For this model we calculate classically the mode spectrum and assume that, due to small nonparabolic terms, these higher modes become observable without changing the mode spectrum significantly. Screening is treated on the same footing as by Fetter. Our classical calculation allows us to determine the complete mode spectrum of systems with parabolic confinement. This information, which is very important for the interpretation of the experiments, was not available from the earlier quantum-mechanical treatments[8,9]

and random phase approximation (RPA) calculations.[15] We find that the calculated frequency ratio of the higher modes agrees very well with experiment for quantum-dot samples containing $N=200$ electrons.

The parabolic confining potential is

$$V(r)=V_0+\tfrac{1}{2}kr^2 , \tag{2}$$

and has a 2D density distribution (see below),

$$n(r)=n(0)(1-r^2/R^2)^{1/2} . \tag{3}$$

Here V_0 and k characterize the potential and $n(0)$ is the electron density in the center of the disk.

The actual experimental structures that will be discussed here and compared with our theory consist of 500 nm$\times$500 nm deep-mesa-etched $Al_xGa_{1-x}As$-GaAs boxes with rounded (radius $\approx$100 nm) corners. The electrons are confined in the middle of the boxes by remote donors in the $Al_xGa_{1-x}As$ and by charged surface states at the etched side walls. The latter separate the electrons from the geometrical edges by a large lateral depletion length of about 150 nm. Thus, the confinement is electrostatic and the parabolic confinement is actually quite a suitable assumption. Nevertheless it is worthwhile to consider for comparison also quantum dots with the abrupt density profile $n(r)$ [Eq. (1)].

II. EQUILIBRIUM PROPERTIES OF AN INDIVIDUAL ELECTRON DISK

A. Classical situation

Let us consider first the classical situation, when the total number of electrons in a dot, N, is large enough so that

$$N\gg 1 . \tag{4}$$

Under these conditions the equilibrium density distribution $n(r)$ follows from the equilibrium condition

$$V(r)+e\varphi(r)=E_F , \tag{5}$$

$$\varphi(r)=\frac{e}{\epsilon}\int_0^{2\pi}d\Theta\int_0^R dr_1\frac{n(r_1)r_1}{|\mathbf{r}-\mathbf{r}_1|} , \tag{6}$$

$$2\pi\int_0^R n(r)dr=N . \tag{7}$$

Here ϵ is the dielectric constant, E_F is the position of the Fermi level. The solution of Eq. (5) with $V(r)$ from (2) gives $n(r)$ [Eq. (3)], with

$$n(0)=\frac{3N}{2\pi R^2},\quad R^3=\frac{3\pi}{4}\frac{e^2}{\epsilon k}N , \tag{8}$$

$$E_F-V_0=N^{2/3}\left[\left(\frac{3\pi e^2}{4\epsilon}\right)^2 k\right]^{1/3} . \tag{9}$$

Certainly the classical distribution $n(r)$ has the form presented in (3) and (8) if the temperature is $T=0$.

B. Thomas-Fermi approximation

To estimate the quantum corrections, we use the Thomas-Fermi approximation. In this case, the equilibrium condition has the form

$$V(r)=e\varphi(r)+\frac{\pi\hbar^2}{2m^*}n(r)=E_F . \tag{10}$$

Here $V(r)$ is from (2), $\varphi(r)$ is from (6), and m^* is the electron effective mass.

We rewrite (10) in terms of dimensionless variables and have

$$V(r)\frac{\epsilon R}{e^2N}+\int_0^1\frac{\tilde{n}(\tilde{r}')}{|\tilde{r}-\tilde{r}'|}d^2\tilde{r}'+\frac{\pi}{2}\frac{a_B}{R}\tilde{n}(\tilde{r})=\text{const} ,$$

$$\tilde{r}=\frac{r}{R},\quad \tilde{n}=n\frac{R^2}{N} . \tag{11}$$

Here $a_B=\epsilon\hbar^2/m^*e^2$ is the Bohr radius. Thus quantum corrections are small if

$$a_B/R\ll 1 . \tag{12}$$

In Ref. 3 the ratio a_B/R is small, i.e., 4×10^{-2} for a dot (a) with $N=200$ electrons and $R=160$ nm and 10^{-1} for a dot (b) with $N=25$ electrons and $R=100$ nm. So, in first approximation, quantum corrections can be neglected.

III. CLASSICAL PLASMA OSCILLATIONS

The problem of classical plasma oscillations can be formulated as the following eigenvalue problem for the electropotential $\varphi(x,y,z,t)$ in a given plasma mode:

$$\varphi(x,y,z,t)=\varphi(x,y,z)e^{-i\omega t} , \tag{13}$$

$$\Delta\varphi=0 , \tag{14}$$

$$-\left.\frac{\partial\varphi}{\partial z}\right|_{z=0}=\begin{cases}2\pi e\,\delta n(x,y)/\epsilon, & x^2+y^2\le R^2\\ 0, & x^2+y^2\ge R^2\end{cases} , \tag{15}$$

$$e\,\delta n(x,y)=-(i\omega)^{-1}\frac{\partial j_i}{\partial x_i},\quad j_i=\sigma_{ik}(r,H,\omega)E_k , \tag{16}$$

$$E_k=-\frac{\partial\varphi}{\partial x_k},\quad x_1=x,\quad x_2=y,\quad i,k=1,2 ,$$

$$\sigma_{ik}(r,H,\omega)=\sigma^0_{ik}(H,\omega)(1-r^2/R^2)^{1/2} , \tag{17}$$

$$\delta n\ll n(r),\quad r\le R . \tag{18}$$

Here the electron disk with density distribution $n(r)$ [Eq. (3)] is in the (x,y) plane, the magnetic field $\mathbf{H}$ is directed along the z direction, $\delta n(x,y,t)$ is the density perturbation, ω is the frequency, j_i is the ith component of the electron current in a disk, and $\sigma^0_{ik}(H,\omega)$ is the corresponding conductivity in the center of the disk. The radial dependence in the determination $\sigma_{ik}(r,H,\omega)$ [Eq. (17)] corresponds to the classical determination of $n(r)$ in Eq. (3).

The variables in the system (13)–(18) can be separated in elliptical coordinates,

$$[\varphi(x,y,z)]_{j,m}=\varphi_{j,m}(\sigma,\tau,\Theta)=P_j^{|m|}(\tau)Q_j^{|m|}(i\sigma)e^{im\Theta} ,$$

$$0\le\tau\le 1,\quad 0\le\sigma<\infty,\quad j\ge m , \tag{19}$$

$$x = R\,[(1+\sigma^2)(1-r^2)]^{1/2}\cos\Theta\ ,$$
$$y = R\,[(1+\sigma^2)(1-\tau^2)]^{1/2}\sin\Theta\ , \tag{20}$$
$$z = R\sigma\tau\ ,$$

where $P_j^{|m|}(x)$ and $Q_j^{|m|}(x)$ are Legendre functions of the first and second kind, respectively.

Using these variables and the determination of σ_{ik}^0(17) in a Drude model,

$$\sigma_{xx}^0 = \frac{i\omega n(0)e^2}{m^*(\omega^2-\omega_c^2)},\quad \sigma_{xy}^0 = \frac{\omega_c n(0)e^2}{m^*(\omega^2-\omega_c^2)}\ ,$$
$$\omega_c = \frac{eH}{m^*c}\ ,$$

we have, from (13)–(19),[17]

$$\omega_{j,m}^2 - \{\omega_c^2 + [j(j+1)-m^2]\Omega_{j,m}^2\} = m\frac{\omega_c}{\omega_{j,m}}\Omega_{j,m}^2\ , \tag{21}$$

$$\Omega_{j,m}^2 = \frac{2\pi e^2 n(0)}{\epsilon m^* R L_{j,m}}\ ,$$
$$L_{j,m} = \frac{2\Gamma((j+m)/2+1)\Gamma((j-m)/2+1)}{\Gamma((j+m)/2+\frac{1}{2})\Gamma((j-m)/2+\frac{1}{2})}\ . \tag{22}$$

Here, $\Gamma(x)$ is the gamma function; $j-m$ is an even integer. If $\sigma_{xx}=0$, we find, from (21) and (22) the result of Tal'yanskiĭ,[18]

$$\omega_{j,m}^2 = \frac{2\pi\sigma_{xy}}{\epsilon R L_{j,m}}m\ . \tag{23}$$

In the limit $\sigma_{xy}=0$, the dispersion law (21) and (22) coincides with the one from Ref. 17:

$$\omega_{j,m}^2 = \frac{2\pi n(0)e^2}{\epsilon m^* R L_{j,m}}[j(j+1)-m^2]\ . \tag{24}$$

General properties of the dispersion law (22) have been discussed in Ref. 17. But in the experimental situation (Ref. 3), the really interesting part of this dispersion follows from (22) with the additional condition

$$j = m\ . \tag{25}$$

As a result, we find

$$\omega_{j,j}^{\pm} = \sqrt{j\Omega_{j,j}^2 + \omega_c^2/4} \pm \omega_c/2\ . \tag{26}$$

The three lowest modes, $\omega_{11}^{\pm}$, $\omega_{22}^{\pm}$, and $\omega_{33}^{\pm}$, are depicted in Fig. 1. From (26), (22), and (8), we can first determine the frequency of the lowest plasmon mode and (at $H=0$) find

$$\omega_{11}^2 = k/m^*\ . \tag{27}$$

This important result shows that for the harmonic confinement the frequency ω_{11} does only depend on the curvature of the bare external confining potential. It is not sensitive to the number of electrons, N, and the static one-particle screening, if many electrons are "filled" into the dots. The same results have also been obtained classically for quantum-wire structures[20] and quantum mechanically for quantum wells with parabolic confinement[8] and quantum dots.[9,21] The quantum-mechanical calculations show that this statement is also correct, with inclusion of quantum corrections. The quantum-mechanical calculations[8,9] only provide the lowest, the dipole, mode ω_{11}. Our calculation also determine the frequencies of the higher modes which is important for the interpretation of the experimental results. We express these frequencies as the ratios of ω_{22} and ω_{33} relative to ω_{11}:

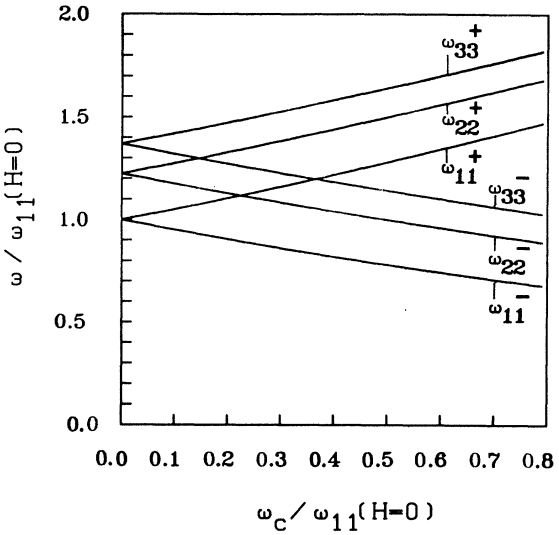

FIG. 1. The three lowest eigenmodes, $\omega_{11}^{\pm}$, $\omega_{22}^{\pm}$, and $\omega_{33}^{\pm}$, of a quantum dot with parabolic confinement.

$$\omega_{22}^2/\omega_{11}^2 = 3/2 \quad\text{and}\quad \omega_{33}^2/\omega_{11}^2 = 15/8\ . \tag{28}$$

These ratios are not sensitive to the radius of the disk, R, nor to the total number of electrons, N. [Note that in a quantum-mechanical treatment beyond Refs. 8 and 9, one expects that, if for an infinitely small perturbation of the harmonic confinement coupling to higher modes becomes allowed, $\omega_{22}=2\omega_{11}$ is only correct for one electron per dot. Already for $n=2$ electrons, ω_{22}/ω_{11} decreases and approaches, with increasing number of electrons, the classical limit (28).]

From (26) we find that with increasing magnetic field all modes split into two resonances, one with positive, the other with negative H dispersion (see Fig. 1). This leads to a mode crossing, e.g., crossing between the ω_{33}^- and ω_{11}^+ mode occurs at H^* with a corresponding cyclotron frequency ω_c^*. At the crossing point, we have the condition [see (26)]

$$\left[\omega_{33}^2(H=0)+\frac{\omega_c^{*2}}{4}\right]^{1/2} - \frac{\omega_c^*}{2} = \left[\omega_{11}^2(H=0)+\frac{\omega_c^{*2}}{4}\right]^{1/2} + \frac{\omega_c^*}{2}$$

or

$$\Delta^2=\frac{\omega_c^{*2}}{\omega_{11}^2(H=0)} =\frac{\left[\frac{\omega_{33}^2(H=0)}{\omega_{11}^2(H=0)}-1\right]^2}{2\left[\frac{\omega_{33}^2(H=0)}{\omega_{11}^2(H=0)}+1\right]}=0.133 . \quad (29)$$

The crossing frequency $\omega_{33,11}$ is equal to

$$\frac{\omega_{33,11}}{\omega_{11}(H=0)}=\left[1+\frac{\Delta^2}{4}\right]^{1/2}+\frac{\Delta}{2}=1.20 . \quad (30)$$

The corresponding position of the crossing frequency $\omega_{33,11}$ between $\omega_{33}^{-}(H)$ and $\omega_{11}^{+}(H)$ in the case of the abrupt density profile, $n(r)$ from (1), is [see Fig. 1(c) of Ref. 16]

$$\frac{\omega_{33,11}}{\omega_{11}(H=0)}=1.35 . \quad (31)$$

The numbers obtained with (30) and (31) are quite different. So the ratio $\omega_{33,11}/\omega_{1i}(H=0)$ can be used to analyze the equilibrium density distribution $n(r)$ in a quantum dot.

IV. COMPARISON WITH EXPERIMENTS

Symmetry considerations, similarly as given below, show that for a harmonic confining potential, (2) and (3), a uniform high-frequency field (dipole excitation) can only excite the mode with $j=m=1$. In the experiments in Ref. 3 also higher modes are observed. Possible origins for such excitations are (a) deviations from a circular shape of the actual quantum dots. The nominal geometry of the dots in Ref. 3 is a squarelike one with rounded corners. As a result the general expansion of the confining potential $V(r)$ should contain the angular dependence

$$V(r,\Theta)=V_0+\tfrac{1}{2}kr^2+\tfrac{1}{4}qr^4+\tfrac{1}{4}qr^4\cos(4\Theta) . \quad (32)$$

For this angular dependence of $V(r,\Theta)$, the coupling between ω_{11} and ω_{33} modes becomes possible. The matrix element

$$\langle\varphi_{11}(r,\Theta)|V(r,\Theta)|\varphi_{33}(r,\Theta)\rangle \propto\int_0^{2\pi}\cos\Theta\cos(3\Theta)\cos(4\Theta)d\Theta\neq 0 \quad (33)$$

is nonzero and this is a possible explanation for coupling between the modes ω_{11} and ω_{33}. The mode ω_{22}, however, does not couple for the potential (32). The same reasons ($\langle\varphi_{11}|V|\varphi_{33}\rangle\neq 0$) can be used for the interpretation of the experimentally observed anticrossing[3] between modes ω_{11} and ω_{33} in a magnetic field. But in this case, the perturbation theory above should be modified. Another possible origin for the excitation of higher-index modes are (b) interactions between dots, e.g., if these are arranged in a quadratic array and (c) deviation from a parabolic confinement. It has been shown[21] that, even for a circularly shaped potential, coupling to higher modes becomes possible if, e.g., r^6 terms are included in the potential. Under such conditions, the anticrossing behavior that is observed in the experiments[3] can also be explained, at least qualitatively. Experimental evidence, i.e., the fact that the strength of the anticrossing increases with decreasing dot radius, suggests that this last effect, (c), is the dominant contribution (see Ref. 3 and for more details Ref. 4).

In the experiments[3] there is a possibility to determine without any fitting directly the value $\omega_{11}(H=0)$ and the position of the crossing point, $\omega_{33,11}$. For the two samples one finds

$$\text{(a) } (R=160\text{ nm}, N=200)\ \frac{\omega_{33,11}}{\omega_{11}(H=00)}=1.25 , \quad (34)$$

$$\text{(b) } (R=100\text{ nm}, N=25)\ \frac{\omega_{33,11}}{\omega_{11}(H=0)}=1.5 . \quad (35)$$

Using these experimental numbers and the determinations (30) and (31) we can see that the frequency ratio of sample (a) with $N=200$ agrees very well with our parabolic model. Sample (b), however, has a significantly different mode spacing.

We finally would like to give expressions for the radii in the two approximations. For the parabolic case, the radius R can be estimated, using the relations ω_{11} [Eq. (27)] and R [Eq. (8)],

$$R^3=\frac{3\pi}{4}\frac{e^2N}{\epsilon k}=\frac{3\pi e^2N}{4\epsilon m^*\omega_{11}^2} . \quad (36)$$

For the abrupt-density-profile approximation, we have[16]

$$R=\frac{2\pi e^2 n_s}{m^*\epsilon\omega_{11}^2(H=0)},\quad n_s=\frac{N}{\pi R^2} . \quad (37)$$

In our calculations, we have neglected dissipation. This is justified for the experiments in Ref. 3 since there one always observes sharp resonances and has thus the high-frequency condition $\omega\tau\gg 1$. In this case, dissipation can be introduced within a Drude model. The formulation is well known for the lowest mode.[10] In the high-frequency regime, dissipation determines the linewidth and causes a very small frequency shift, which can be neglected for the interpretation. Dissipation causes interesting filling-factor-dependent effects in the low-frequency regime and under quantum Hall-effect conditions.[22] However, in the experiments in Ref. 3, there is no filling-factor-dependent feature both in resonance position and linewidth, and so we have not treated these effects here.

It is clear that, beyond our model, for smaller structures deviations from the parabolic confinement and quantum corrections ($R\approx a_B$) must be treated on the same level of approximation, in particular to explain the experimentally observed anticrossing and the different mode spacing in the smaller dots [sample (b)]. However, such treatment is a very difficult task and also not available so far from fully numerical calculations in a system with a small number of electrons.[9] Such effects are beyond the scope of our paper.

V. CONCLUSIONS

We have calculated the equilibrium properties and the complete excitation spectrum of the dynamic response for an electron disk starting from a classical electron system in a harmonic-oscillator potential. Our theory explains the resonance frequencies of different experimentally observed modes in dot structures containing $N > 200$ electrons in a disk of radius $R > 160$ nm.

*On leave from Institute of Solid State Physics, 142 432 Cernogolovka, Moscow District, U.S.S.R.

[1]K.-F. Berggren, T. J. Thornton, D. J. Newson, and M. Pepper, Phys. Rev. Lett. **57**, 1769 (1986).

[2]Ch. Sikorski and U. Merkt, Phys. Rev. Lett. **62**, 12 164 (1989).

[3]T. Demel, D. Heitmann, P. Grambow, and K. Ploog, Phys. Rev. Lett. **64**, 788 (1990).

[4]T. Demel, D. Heitmann, P. Grambow, and K. Ploog, in *Proceedings of the 6th International Winter School on Localization and Confinement of Electrons in Semiconductors, Mauterndorf, 1990,* edited by G. Bauer, H. Heinrich, and F. Kuchar (Springer-Verlag, Heidelberg, 1991), p. 51.

[5]T. Demel, D. Heitmann, P. Grambow, and K. Ploog, Appl. Phys. Lett. **33**, 2176 (1988).

[6]T. Demel, D. Heitman, P. Grambow, and K. Ploog, Phys. Rev. B **38**, 12 732 (1988).

[7]A. Kumar, S. E. Laux, and F. Stern, Phys. Rev. B **42**, 5166 (1990).

[8]L. Brey, N. Johnson, and P. Halperin, Phys. Rev. B **40**, 10 647 (1989).

[9]P. A. Maksym and T. Chakraborty, Phys. Rev. Lett. **65**, 108 (1990).

[10]S. J. Allen, H. L. Störmer, and J. C. Hwang, Phys. Rev. B **28**, 4875 (1983).

[11]D. C. Glattli, E. Y. Andrei, G. Deville, J. Poitrenand, and F. I. B. Williams, Phys. Rev. Lett. **54**, 1710 (1985).

[12]D. B. Mast, A. J. Dahm, and A. L. Fetter, Phys. Rev. Lett. **54**, 1706 (1985).

[13]S. Govorkov, M. Resnikov, A. Senichkov, and V. I. Tal'yanskiĭ, Pis'ma Zh. Eksp. Teor. Fiz. **44**, 380 (1986) [JETP Lett. **44**, 487 (1986)].

[14]V. Volkov, D. Galchenkov, and L. Galchenkov, Pis'ma Zh. Eksp. Teor. Fiz. **44**, 510 (1986) [JETP Lett. **44**, 665 (1986)].

[15]W.-M. Que and G. Kirczenow, Phys. Rev. B **38**, 3614 (1988).

[16]A. Fetter, Phys. Rev. B **33**, 5221 (1986).

[17]S. Nazin and V. Shikin, Fiz. Nizk. Temp. **15**, 227 (1989) [Sov. J. Low Temp. Phys. **15**, 127 (1989)].

[18]V. I. Tal'yanskiĭ, Pis'ma Zh. Eksp. Teor. Fiz. **43**, 96 (1986) [JETP Lett. **43**, 127 (1986)].

[19]R. P. Leavitt and J. W. Little, Phys. Rev. B **34**, 2450 (1986).

[20]V. Shikin, D. Heitmann, and T. Demel, Zh. Eksp. Teor. Fiz. **96**, 1406 (1989) [Sov. Phys. JETP **69**, 797 (1989)]; Surf. Sci. **229**, 276 (1990).

[21]R. R. Gerhardts (unpublished).

[22]E. Y. Andrei, D. C. Glattli, F. I. B. Williams, and M. Heiblum, Surf. Sci. **196**, 501 (1988).